Distributed Multi-Target Tracking for Heterogeneous Mobile Sensing Networks with Limited Field of Views

Jun Chen and Philip Dames

***Abstract*— This paper introduces the *normalized unused sensing capacity* to measure the amount of information that a sensor is currently gathering relative to its theoretical maximum. This quantity can be computed using entirely local information and works for arbitrary sensor models, unlike previous literature on the subject. This is then used to develop a distributed coverage control strategy for a team of heterogeneous sensors that automatically balances the load based on the current unused capacity of each team member. This algorithm is validated in a multi-target tracking scenario, yielding superior results to standard approaches that do not account for heterogeneity or current usage rates.**

I. Introduction

Multiple target tracking (MTT) is a broad class of problems that includes applications ranging from environmental monitoring to surveillance to smart cities. In recent years, MTT problems are increasingly being solved by mobile sensing networks, due to their capability to reactively adjust sensor coverage over the mission space as new information is collected. Developing algorithms to determine and achieve the desired sensor states is the problem of coverage control, which aims to maximize some total measure of the team's performance over the entire mission space.

We choose to utilize a distributed algorithm, as these scale well to larger sensing networks and are more tolerant of individual failures. The most widely used distributed coverage control strategy in recent years are Voronoi-based methods [1]–[4]. The basic idea is to partition an environment using the Voronoi tessellation and then recursively drive each sensor towards the weighted centroid of its Voronoi cell, a process known as Lloyd's algorithm [5]. This will eventually achieve a local maximum of the global measure of team performance. In these algorithms, sensors are only required to communicate with their direct neighbors and it is typically assumed that sensors have perfect knowledge of their locations and that the mission space is convex. A number of recent works have provided various solutions to accommodate uncertainty in sensor location [6]–[9] and to allow for non-convex spaces [10]–[13].

None of the above approaches consider heterogeneity in the team, which limits their use in complex scenarios where a variety of different types of robots and sensors may be needed to complete the task. Weighted Voronoi diagrams, which include power diagrams, have recently been used to account for heterogeneity in the radii of circular sensor footprints [13]–[16] and energy levels [17]. Voronoi-based methods have also been used for wedge-shaped sensor field of views (FoV) [18]. Stergiopoulos and Tzes [19]–[21] used novel partitioning and distribution algorithms for sensing networks where all sensor FoVs share the same arbitrary shape (but may be of a different size). Hexsel *et al.* [22] introduced a gradient ascent-based coverage control algorithm to maximize the joint probability of detection in anisotropic sensing networks. However, as with most gradient ascent approaches, sensors can prematurely converge to a local extremum of the objective function. This is especially harmful in target tracking scenarios, since this often results in multiple sensors tracking the same target while others are left unobserved.

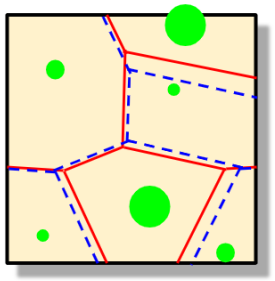

Fig. 1. Comparison of a Voronoi diagram (red solid lines) and a power diagram (blue dotted lines) with 6 cells. The size of each generator points (green disks) for the power diagram corresponds to its power radii (weights). A power diagram is equivalent to a Voronoi diagram when the weights for all generator points are identical.

Our approach is based on a novel measure, the *normalized unused sensing capacity*, which measures the difference between the current information that a sensor gathers and the theoretical maximum. This can be computed using entirely local information and does not require any assumptions about the type of sensor or the shape of the sensor field of view. We then use this measure to construct a power diagram. In this way, the task load for each individual robot is automatically balanced with its neighbors, assigning robots that have more accurate sensors, larger sensor fields of view, and/or are not currently tracking any objects to cover larger areas. We demonstrate the efficacy of this approach through a series of simulated experiments, showing that our approach yields higher quality and more reliable tracking in teams with large amounts of heterogeneity.

II. Problem Formulation

We assume that we have a team of n mobile sensors $S = \{s_1, s_2, ...s_n\}$ with positions $Q = \{q_1, \ldots, q_n\}$ and

*This work was supported by NSF Grant IIS-1830419.

J. Chen and P. Dames are with the Department of Mechanical Engineering, Temple University, Philadelphia, PA 19122, USA {jchen,pdames}@temple.edu

orientations $\Theta = \{\theta_1, \ldots, \theta_n\}$. Each sensor is kinematic, following the dynamical model:

$$\begin{aligned} \dot{q_i} &= u_i, \\ \dot{\theta_i} &= v_i, \end{aligned} \tag{1}$$

where u_i and v_i are the control inputs for position and orientation respectively of the ith sensor. The team is tasked to search for and track targets in a convex environment $E \subset R^2$, though there are several existing methods to incorporate obstacles and concavity [10]–[13].

A. Lloyd's Algorithm

The objective of Lloyd's algorithm is to minimize the following functional:

$$\mathcal{H}(Q, \mathcal{W}) = \sum_{i=1}^{n} \int_{\mathcal{W}_i} f\big(\|x - q_i\|\big)\phi(x)dx, \tag{2}$$

where $\mathcal{W}_i$ is dominance region of sensor s_i (*i.e.*, the region that sensor s_i is responsible for), $\|\cdot\|$ is the Euclidean distance, $x \in E$, and $f(\cdot)$ is be a monotonically increasing function. The role of f is to quantify the cost of sensing due to degradation of a sensor's ability to measure events with increasing distance. The dominance regions $\mathcal{W}_i$ form a partition over E, meaning the regions have disjoint interiors and the union of all regions is E [1].

The goal is for the team to minimize the functional (2), both with respect to the partition set $\mathcal{W}$ and the sensor positions Q. Minimizing $\mathcal{H}$ with respect to $\mathcal{W}$ induces a partition on the environment $V_i = \{x \mid i = \arg\min_{k=1,\ldots,n} \|x - q_k\|\}$. In other words, V_i is the collection of all points that are the nearest neighbor of s_i. This is the Voronoi partition, as Figure 1 shows, and these V_i are the Voronoi cells, which are convex by construction. We call q_i the generator point of V_i. Minimizing $\mathcal{H}$ with respect to Q leads each sensor to the weighted centroid of its Voronoi cell [1], that is

$$q_i^* = \frac{\int_{V_i} x\phi(x)\,dx}{\int_{V_i} \phi(x)\,dx}. \tag{3}$$

Lloyd's algorithm sets the control input for sensor s_i to

$$u_i = -k_{\text{prop}}(q_i - q_i^*), \tag{4}$$

where $k_{\text{prop}} > 0$ is a positive gain. The angular velocity uses a bang-bang strategy, maximizing the angular velocity until the sensor is facing directly towards the goal. By following this control law, the sensors asymptotically converge to the weighted centroids of their Voronoi cells. This still holds true when $\phi(x)$ varies with time.

B. Multiple Target Tracking

In an MTT setting, a natural choice for $\phi(x)$ is a target density function. This density function, which changes over times as targets appear, disappear, and move, can be estimated using any number of standard MTT algorithms. Some best known trackers include global nearest neighbor (GNN) [23], joint probabilistic data association (JPDA) [24], multiple hypothesis tracking (MHT) [25], particle filters (PF) [26], and the probability hypothesis density (PHD) filter [27]. Each of these methods use a Bayesian filter to track the multi-target posterior, with the main differences being in how they approach the problem of data association, *i.e.*, matching multiple measurements to target tracks.

In this paper, we use the PHD filter, as it does not require any explicit data association. Recently, we have shown that this works effectively in a distributed MTT problem using a homogeneous team of robots [28]. In [28], we introduce a distributed version of the PHD filter (also used in this paper) and utilize its output as the weighting function $\phi(x)$ in (3). This effectively drives each sensor towards estimated target locations, enabling the team to actively search for and track targets cooperatively in a distributed manner. However, it is important to note that the overall framework presented in this paper can be easily adapted to any other choice of Bayesian MTT tracker.

C. PHD Filter

The PHD filter tracks the first statistical moment (*i.e.,* the mean) of a distribution over random finite sets (RFSs) (*i.e.,* sets with a random number of random elements) [27]. RFSs can be used to represent quantities such as the set of targets in the environment or the measurements received by a robot. The *Probability Hypothesis Density* (PHD), denoted by $v(x)$, is the first order moment of a RFS and takes the form of a density function over the state space of a single target or measurement. The integral of PHD over a region is equal to the expected number of targets in that region numerically at that time. Note that $v(x)$ is *not* a probability density function (PDF), but can converted into one by normalizing by the expected number of targets in a space E,

$$p_t(x|E) = \frac{v(x)}{\int_E v(x)dx}. \tag{5}$$

The PHD filter recursively predicts this target density function using transition probability and updates it with sensor measurements in order to estimate the target set [27]. In this work we represent the PHD using a set of weighted particles [29], a standard approach for nonlinear measurement models.

III. Multi-target Tracking using Heterogeneous Mobile Sensing Networks

We assume that each sensor s_i has a finite field of view (FoV) f_i, but the FoV need not be the same for any sensors. Let $p_d(x|q_i, \theta_i)$ denote the probability of sensor s_i, with current position q_i and orientation θ_i, detecting a target with state $x \in E$. For a sensor with a finite FoV f, $p_d(x)$ is non-zero only when $x \in f$. Examples of f_i include a wedge shape for a camera or a circle for a lidar. We assume that p_d is time-invariant, but make no other assumptions about the shape of f_i or about the functional form of p_d. In practice, p_d can be estimated either via a data driven manner [30] or by experience.

The total detecting capability of sensor s_i is given by

$$D_i = \int_{f_i} p_d(x|q_i, \theta_i)\,dx. \tag{6}$$

Note, D_i measures both the size of f_i and the sensor's ability to detect information within f_i. This will allow us to map the detection model of any arbitrary sensor s_i to a perfect isotropic detection model with the identical sensing capacity.

A. Unused Sensing Capacity

In this paper, we consider sensor heterogeneity in terms of not only sensing capability, such as FoV and detection accuracy, but also its current usage to track targets. When a sensor has detected a target and started to track it, it has less capacity to track other targets than a sensor with no target detected yet.

For each point $x \in f_i$, since targets cannot overlap, at most 1 target can be found at x. Thus, $\max(v(x)) = 1$ and the maximum possible detection probability is given by

$$p_{\max}(x) = p_d(x|q_i, \theta_i) \cdot \max(v(x)) = p_d(x|q_i, \theta_i). \quad (7)$$

Thus, the maximum total possible detection, *i.e.*, s_i's sensing capacity is defined

$$C_{\max,i} = \int_{f_i} p_d(x|q_i, \theta_i)\, dx = D_i. \quad (8)$$

Meanwhile, the expected number of target detections at x is given by

$$p_{\exp}(x) = p_d(x) p_t(x). \quad (9)$$

Thus, the total expected target detection is defined

$$\begin{aligned} C_{\exp,i} &= \int_{f_i} p_d(x|q_i, \theta_i) p_t(x|f_i)\, dx \\ &\overset{(5)}{=} \frac{\int_{f_i} p_d(x|q_i, \theta_i) v(x)\, dx}{\int_{f_i} v(x)\, dx}. \end{aligned} \quad (10)$$

Definition 1 (Normalized Unused Sensing Capacity)**.** The *normalized unused sensing capacity* for sensor s_i, denoted U_i, is given by

$$U_i = C_{\max,i} - C_{\exp,i} = \int_{f_i} \big(1 - \frac{v(x)}{\int_{f_i} v(x)\, dx}\big) p_d(x|q_i, \theta_i)\, dx. \quad (11)$$

Note that (11) can be easily modified when other Bayesian filters are used for tracking, as we discussed in Sec. II-B. The normalized unused sensing capacity quantifies current capacity for a sensor to track targets. A sensor originally with greater detection capability is supposed to have stronger ability to track more targets, but such ability decays as increasing number of targets have been tracked by this sensor.

B. Power Diagram Implementation

Sensor heterogeneity is considered by controlling the spatial deployment of the network over time to reach an optimized total detection probability of targets. This requires optimization of both space partitioning and location in each partition. While a Voronoi diagram generated by sensor locations yields the optimal dominance region V_i for sensor s_i in a homogeneous isotropic sensing network, power diagrams [31] are often used for heterogeneous team. The power diagram is a variant of the standard Voronoi diagram that uses the power distance, $f(\|x-p_i\|) = \|x-p_i\|^2 - \rho_i^2$, where ρ_i is the power radius of s_i and p_i is the generator point, taking Fig. 1 as an example. Previous works that use the power diagram utilized sensor positions as the generator points, p_i, and the radii of the sensor FoVs as the weights, ρ_i, to account for sensor heterogeneity [13], [16], which implicitly limits the approach to isotropic sensors. On the other hand, our approach extends to heterogeneous anisotropic sensors.

1) Optimized Partitions: We utilize the normalized unused sensing capacity U_i to set the power radius for each sensor, a novel strategy to account for the heterogeneity in partitioning the dominance regions. As a result, the distributed optimization functional (2) becomes

$$\mathcal{H}_p(Q, \mathcal{W}) = \sum_{i=1}^{n} \int_{\mathcal{W}_i} \left(\|x - p_i\|^2 - g(U_i)^2\right) \phi(x)\, dx, \quad (12)$$

where $g : \mathbb{R} \to \mathbb{R}$ is a mapping from the measure of sensing capacity to the measure of sensing radius for sensors. Since the normalized unused sensing capacity has units of area, we choose g such that the resulting power radius, $g(U_i)$, is equal to the radius of a perfect (*i.e.,* $p_d = 1$) isotropic sensor with the same total sensing capability, D_i, *i.e.*, $\pi g(U_i)^2 = U_i$. Therefore we have

$$g(U_i) = \sqrt{\frac{U_i}{\pi}}. \quad (13)$$

Existing methods based on the power diagram, such as [13], [16], [17], assume that the sensor's detection probability is a non-increasing function of the distance to the sensor. In other words, the location of a sensor is the location that maximizes the probability of detection of that sensor. Thus, it makes sense that they use the sensor location as the generator point, *i.e.,* let $p_i = q_i$. However, this no longer holds true for anisotropic sensors. Instead, we find the weighted centroid of the detection probability

$$q_{\max,i} = \frac{\int_{f_i} x p_d(x|q_i, \theta_i)\, dx}{\int_{f_i} p_d(x|q_i, \theta_i)\, dx}, \quad (14)$$

which we call the *centroid of detection* (COD). We use these COD, $q_{\max,i}$, as the generator points for our power diagram. Note that in the case of an isotropic sensor the COD will be the same as the sensor position.

Thus, the optimal partition becomes

$$W_i = PV_i = \{x \mid i = \underset{k=1,\dots,n}{\arg\min} (\|x - q_{\max,i}\|^2 - g(U_i)^2)\}. \quad (15)$$

Remark 1. The proposed spatial partitioning strategy maps an arbitrary sensor model to a perfect isotropic sensor in a way that preserves the weighted center of detection $q_{\max,i}$ and the total sensing capacity D_i by choosing the appropriate mapping of the normalized unused sensing capacity $g(U_i)$. By doing that, a sensor's unused sensing capability is mapped to the same scale as the sensing range and thus can be directly compared with the size of the partition.

2) Optimized poses: Similar to [1], at each moment the partial derivative of $\mathcal{H}_p(Q, \mathcal{W})$ w.r.t. $q_{\max,i}$ is given by

$$\frac{\partial \mathcal{H}_p(Q)}{\partial q_{\max,i}} = 2M_{PV_i}(q_{\max,i} - C_{PV_i}), \tag{16}$$

where M_{PV_i} and C_{PV_i} are the mass and center of mass respectively, defined as

$$\begin{aligned} M_{PV_i} =& \int_{PV_i} \phi(x)\, dx, \\ C_{PV_i} =& \frac{1}{M_{PV_i}} \int x\phi(x)\, dx. \end{aligned} \tag{17}$$

Thus, by recursively driving $q_{\max,i}$ to C_{PV_i}, the partial derivative continues to approach to 0 and thus sensing capability of s_i in PV_i is optimized. The control inputs in (1) for s_i is then given by

$$\begin{aligned} u_i =& d(C_{PV_i} - q_{\max,i})(dt)^{-1}, \\ v_i =& \begin{cases} d(\Delta\theta)(dt)^{-1} & \Delta\theta \geq \theta_i \\ d(-\Delta\theta(dt)^{-1} & \text{else} \end{cases}, \\ \Delta\theta =& \text{ang}(C_{PV_i} - q_{\max,i}) - \theta_i, \end{aligned} \tag{18}$$

where $\text{ang}(\cdot)$ denotes the angle of a position vector in global frame. Note that when sensors are homogeneous, the control law (4) yields an identical result as using traditional Lloyd's algorithm in [1].

3) Quantifying Heterogeneity: In order to make quantitative statements about our results, we must first define a measure of the heterogeneity in a team.

Definition 2 (Heterogeneity Level)**.** The *heterogeneity level* of a sensing network $S = \{s_1, s_2, ...s_n\}$, denoted by $L(S)$, is given by standard deviation of the power radius of each sensor in S, *i.e.,*

$$L(S) = \sqrt{\frac{1}{n}\sum_{i=1}^{n}(g(U_i) - \bar{g})^2} \tag{19}$$

where $\bar{g} = \frac{1}{n}\sum_{i=1}^{n} g(U_i)$.

Definition 3 (Total Sensing Capacity)**.** The *total sensing capacity*, of a sensing network S is given by

$$C(S) = \sum_{i=1}^{n} C_{\max,i}. \tag{20}$$

Based on the above definitions, we make the following conjecture.

Conjecture 1. For teams with the same total sensing capacity, $C(S)$, our novel power diagram formula will provide increasing benefits over a standard Voronoi diagram as the heterogeneity, $L(S)$, increases.

IV. Simulation Results

We conduct a set of simulated MTT experiments in MATLAB in order to validate our proposed coverage control law. The following tests using sensors with two wedge-shaped FoVs with angle of view $45°$ and $240°$ respectively for simplicity, as shown in Fig. 2, though there is no limitation of types of shape or numbers of type to implement our methods. For simplicity, we assume that the probability of detection is constant within the field of view

$$p_d(x) = \begin{cases} p_d & x \in f_i \\ 0 & \text{else} \end{cases} \tag{21}$$

We define eight separate sensor classes that we use in the following tests, as is outlined in Table I. Based on these class definitions, we define eight different team compositions, shown in Table II.

Most existing work such as [3], [13], [16]–[19] validated power diagram based methods by presenting the convergence similar to [1], assuming that all sensors have perfect knowledge of $\phi(x)$ in their own cells. In this paper, we estimate $\phi(x)$ online using the PHD filter, a significantly harder challenge. Furthermore, most other works do not make a direct comparison with other approaches, even to traditional Voronoi diagram based methods. We will compare our new approach against the naïve Voronoi based method to provide a baseline of performance.

(a) Type 1 shape (b) Type 2 shape

Fig. 2. Two types of footprint shape used in simulations. Type 1 and type 2 have viewing angles of $45°$ and $240°$ respectively. Black squares represent the location of sensors.

TABLE I
Classes of Heterogeneous Sensors

Class \ Specs	Viewing Angle (deg)	Radius (m)	p_d
A	240	8	0.99
B	45	8	0.99
C	45	8	0.7
D	240	25	0.99
E	45	10	1
F	240	10	1
G	240	14.142	1
H	240	20	1

TABLE II
Team Compositions

Team \ Class	A	B	C	D	E	F	G	H
1	4	12						
2		3	12	8				
3		4	16	12				
4		5	20	15				
5		6	24	18				
6					20			4
7					20		10	
8					20	20		

To measure the tracking performance we use the first order Optimal SubPattern Assignment (OSPA) metric [32], a commonly-used approach in MTT. The error between two sets X, Y, where $|X| = m \leq |Y| = n$ without loss of generality, is

$$d(X,Y) = \left(\frac{1}{n}\min_{\pi\in\Pi_n}\left(\sum_{i=1}^{m} d_c(x_i, y_{\pi(i)})^p + c^p(n-m)\right)\right)^{1/p}, \quad (22)$$

where c is a cutoff distance, $d_c(x,y) = \min(c, \|x-y\|)$, and Π_n is the set of all permutations of the set $\{1, 2, \ldots, n\}$. This gives the average error in matched targets, where OSPA considers all possible assignments between elements $x \in X$ and $y \in Y$ that are within distance c of each other. This can be efficiently computed in polynomial time using the Hungarian algorithm [33]. In our case, the two sets X and Y represent the true and estimated target set and we use the parameters $c = 10\,\mathrm{m}$ and $p = 1$. Note that a *lower* OSPA value indicates a more accurate tracking of the target set.

A. Convergence

We first show results of multi-target search and tracking using proposed coverage control strategy. The environment E is an open $40 \times 40\,\mathrm{m}$ square and there are 8 targets moving inside the mission space with velocity 2 m/s along a fixed heading. We use team composition 1, which has a total of 16 robots, 4 of which have wide FoVs and 12 of which have narrow FoVs. All sensors have a 2 m/s maximum linear velocity and 5 rad/s maximum angular velocity. Figure 3a shows the initial distribution of the sensors and targets.

The sensors begin with a uniform PHD, meaning they have no prior knowledge of the target density distribution, and most targets are not located in any of the sensor FoVs. Figure 3b shows the final distribution after 200 s. All 8 targets are located inside sensor FoVs and around the CODs of sensors, meaning that the team has successfully located and tracked each target. Sensors may either track one target or multiple targets by having their CODs follow the peaks of target density in individual cells. Other sensors are distributed over the empty space to cover the entire search space in order to find any untracked sensors.

Figure 3c shows trajectories of targets and sensor CODs over the entire 200 s. Note that trajectories of CODs are different from trajectories of sensor locations. Targets are tracked by sensor CODs via sensors' active control of their positions and orientations so that areas with high target density can be detected with sensors' highest detection likelihood. Most of the targets are initially not tracked but end up being tracked, as most of blue lines are not followed by green lines near the start locations but then been followed near their end locations. It is also shown that trajectories of CODs distribute across the entire mission space, which presents the coverage efficacy of the proposed control law.

B. Power Diagram Efficacy

Next, we demonstrate the efficacy of utilizing power diagram weighted by $g(U)$ for assigning dominance regions. In these tests the environment E is larger, at $100 \times 100\,\mathrm{m}$. Targets again move at 2 m/s, but this time their heading directions randomly change over time. Unlike IV-A, where targets moved inside the mission space, in these tests targets may enter or leave the environment by crossing over the boundary. This means that the number of targets varies over time, and the true number of targets is not known to the sensors. Initially, there are 30, 40, or 50 targets within the environment. We compare four different team compositions, 2, 3, 4, and 5, each of which is composed of the same sensor types in the same ratio, as shown in Table II. For each initial number of targets and each team composition, we run 10 trials using our method and another 10 trials using a standard Voronoi diagram, with each trial lasting for 1000 s. All sensors have 2 m/s maximum linear velocity and 5 rad/s maximum angular velocity. The sensors and targets are randomly distributed in the mission space at the beginning of each trial.

Figure 4 shows the results of these trials. We plot the average OSPA error of the last 800 s for each trial, to present the steady state tracking accuracy. The first thing to note is that larger teams yield better tracking performance, which is quite intuitive. Also, as we expected, the power diagram methods consistently yields superior tracking accuracy to Voronoi diagram methods across all team sizes and target numbers. The results confirm the efficacy of using power diagram for locational optimization for heterogeneous sensing networks. Power diagrams optimize the spatial partitioning by assign larger dominance regions to sensors with more unused sensing capacity and shrink cells for those who have less. As a result, sensing networks account for the variety of sensing capabilities across the team and avoid overloading sensors that are already tracking targets. Therefore, the total detection probability for sensing networks has been optimized.

In addition to decreasing the average tracking error, the power diagram also decreases the range of tracking errors. In other words, sensing networks that use the power diagram have both better and more reliable behavior. This is due to the fact that the optimized assignment of dominance region reduces the probability of targets being lost during tracking.

C. Comparison of Heterogeneity Levels

Lastly we run a series of tests to validate Conjecture 1. We use teams 6, 7, and 8 from Table II, all of which have an identical total sensing capacity (20). The heterogeneity levels, computed using (19), of each team are $L(S_6) = 1.156\,\mathrm{m}$ (which we call level 1), $L(S_7) = 1.889\,\mathrm{m}$ (level 2), and $L(S_8) = 2.384\,\mathrm{m}$ (level 3). The remainder of the simulation parameters are identical to Sec. IV-B and we use 30 initial targets.

Figure 5 shows the average OSPA errors over 10 trials, using data from the last 800 s of each trial. We found a significant improvement in tracking accuracy while using

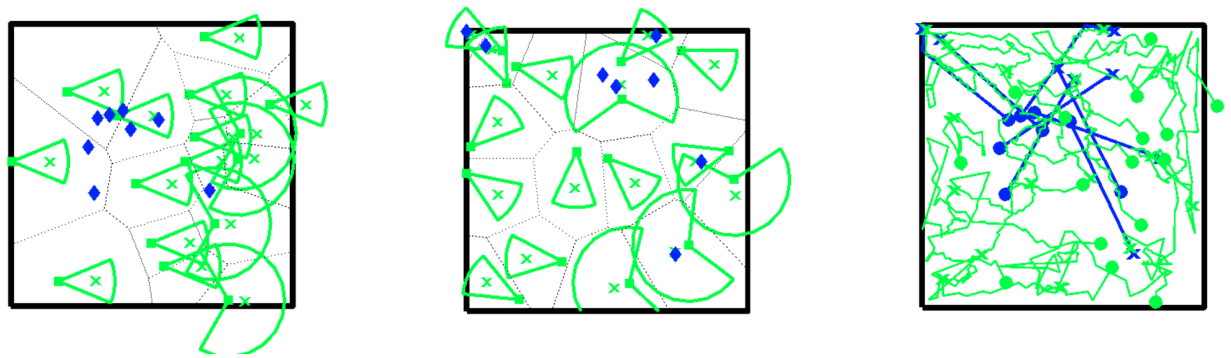

(a) Start (b) End (c) Trajectories

Fig. 3. Figures showing 16 sensors searching for and tracking 8 moving objects over 200 s. Sensors are shown in green squares with green wedges showing their footprints. Green crosses show CODs of each sensor. Power cells are shown in dotted lines. Blue diamonds show target positions. Figures (a) and (b) shows the start and end patterns respectively. Figure (c) shows the trajectories of sensor CODs and targets, using green and blue lines respectively. Starting positions are indicated by circles and the ends by crosses.

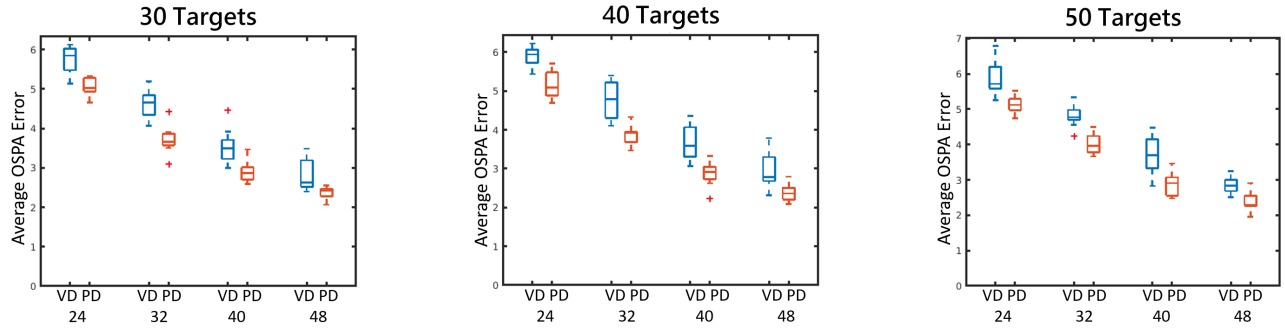

(a) 30 Targets (b) 40 Targets (c) 50 Targets

Fig. 4. Boxplots showing the average OSPA error for each test configuration. Blue and red boxplots show results of using Voronoi diagram and power diagram respectively. Figure 4a, 4b and 4c show results of tracking 30, 40, 50 targets respectively. There are four teams on each boxplot, with 24, 32, 40 and 48 total sensors, respectively from left to right.

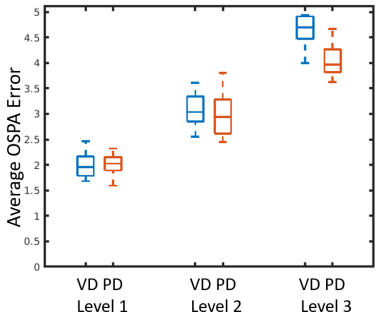

Fig. 5. Boxplot showing the OSPA errors under heterogeneity levels 1-3 from left to right. Blue and red boxplots show results of using Voronoi diagram and power diagram respectively.

power diagram for S_8, which has the highest level of heterogeneity. At the same time, level 2 shows a slight advantage of using power diagram while level 3 presents no improvements. These results summarize our hypothesis in Conjecture 1 . The increase of tracking accuracy by using S_6, S_7 and S_8 is consistent with the change of number of sensors in networks, which affects the mobility for a network. Note also that the heterogeneity level in teams 2–5 is higher than for any of teams 6–8, which is why the differences between the power and Voronoi diagrams are less pronounced in these tests.

V. Conclusions

We propose a distributed coverage control scheme for heterogeneous mobile to track an unknown and time-varying number of targets. This novel strategy allows sensors to have arbitrary sensing models (with limited field of views) and dynamically optimizes the workload for each individual. To do this, we introduce the normalized unused sensing capacity and use this to construct a power diagram to recursively find optimized sensor locations as measurements being updated. Also different from past work, we use the centroid of detection for each sensor as the generator point for the power diagram, allowing each sensor to center its field of view on the area with the most information. Simulation results show the convergence of our proposed method in target tracking scenarios. We also see that our method yields better and more reliable tracking performance compared to a standard Voronoi diagram that does not account for heterogeneity. We also found that this difference increases as the heterogeneity in the team's sensing capabilities increases.

REFERENCES

[1] J. Cortes, S. Martinez, T. Karatas, and F. Bullo, "Coverage control for mobile sensing networks," *IEEE Transactions on Robotics and Automation*, vol. 20, no. 2, pp. 243–255, 2004.

[2] M. Schwager, D. Rus, and J.-J. Slotine, "Decentralized, adaptive coverage control for networked robots," *The International Journal of Robotics Research*, vol. 28, no. 3, pp. 357–375, 2009.

[3] Y. Kantaros and M. M. Zavlanos, "Distributed communication-aware coverage control by mobile sensor networks," *Automatica*, vol. 63, pp. 209–220, 2016.

[4] A. Pierson and D. Rus, "Distributed target tracking in cluttered environments with guaranteed collision avoidance," in *2017 International Symposium on Multi-Robot and Multi-Agent Systems (MRS)*. IEEE, 2017, pp. 83–89.

[5] S. Lloyd, "Least squares quantization in PCM," *IEEE Transactions on Information Theory*, vol. 28, no. 2, pp. 129–137, 1982.

[6] S. Papatheodorou, A. Tzes, K. Giannousakis, and Y. Stergiopoulos, "Distributed area coverage control with imprecise robot localization: Simulation and experimental studies," *International Journal of Advanced Robotic Systems*, vol. 15, no. 5, p. 1729881418797494, 2018.

[7] H. Zhu and J. Alonso-Mora, "B-UAVC: Buffered uncertainty-aware Voronoi cells for probabilistic multi-robot collision avoidance," in *2019 International Symposium on Multi-Robot and Multi-Agent Systems (MRS)*. IEEE, 2019, pp. 162–168.

[8] M. Wang and M. Schwager, "Distributed collision avoidance of multiple robots with probabilistic buffered voronoi cells," in *2019 International Symposium on Multi-Robot and Multi-Agent Systems (MRS)*. IEEE, 2019, pp. 169–175.

[9] J. Chen and P. Dames, "Distributed and collision-free coverage control of a team of mobile sensors using the convex uncertain voronoi diagram," in *2020 American Control Conference (ACC)*. IEEE, 2020, pp. 5307–5313.

[10] J. M. Palacios-Gasós, Z. Talebpour, E. Montijano, C. Sagüés, and A. Martinoli, "Optimal path planning and coverage control for multi-robot persistent coverage in environments with obstacles," in *2017 IEEE International Conference on Robotics and Automation (ICRA)*. IEEE, 2017, pp. 1321–1327.

[11] S. Bhattacharya, R. Ghrist, and V. Kumar, "Multi-robot coverage and exploration on Riemannian manifolds with boundaries," *The International Journal of Robotics Research*, vol. 33, no. 1, pp. 113–137, 2014.

[12] A. Breitenmoser, M. Schwager, J.-C. Metzger, R. Siegwart, and D. Rus, "Voronoi coverage of non-convex environments with a group of networked robots," in *2010 IEEE International Conference on Robotics and Automation*. IEEE, 2010, pp. 4982–4989.

[13] L. C. Pimenta, V. Kumar, R. C. Mesquita, and G. A. Pereira, "Sensing and coverage for a network of heterogeneous robots," in *2008 47th IEEE Conference on Decision and Control*. IEEE, 2008, pp. 3947–3952.

[14] Y. Kantaros, M. Thanou, and A. Tzes, "Distributed coverage control for concave areas by a heterogeneous robot–swarm with visibility sensing constraints," *Automatica*, vol. 53, pp. 195–207, 2015.

[15] N. Bartolini, T. Calamoneri, T. F. La Porta, and S. Silvestri, "Autonomous deployment of heterogeneous mobile sensors," *IEEE Transactions on Mobile Computing*, vol. 10, no. 6, pp. 753–766, 2010.

[16] O. Arslan and D. E. Koditschek, "Voronoi-based coverage control of heterogeneous disk-shaped robots," in *2016 IEEE International Conference on Robotics and Automation (ICRA)*. IEEE, 2016, pp. 4259–4266.

[17] A. Kwok and S. Martinez, "Deployment algorithms for a power-constrained mobile sensor network," *International Journal of Robust and Nonlinear Control: IFAC-Affiliated Journal*, vol. 20, no. 7, pp. 745–763, 2010.

[18] K. Laventall and J. Cortés, "Coverage control by robotic networks with limited-range anisotropic sensory," in *2008 American Control Conference*. IEEE, 2008, pp. 2666–2671.

[19] Y. Stergiopoulos and A. Tzes, "Autonomous deployment of heterogeneous mobile agents with arbitrarily anisotropic sensing patterns," in *2012 20th Mediterranean Conference on Control & Automation (MED)*. IEEE, 2012, pp. 1585–1590.

[20] ——, "Spatially distributed area coverage optimisation in mobile robotic networks with arbitrary convex anisotropic patterns," *Automatica*, vol. 49, no. 1, pp. 232–237, 2013.

[21] ——, "Cooperative positioning/orientation control of mobile heterogeneous anisotropic sensor networks for area coverage," in *2014 IEEE International Conference on Robotics and Automation (ICRA)*. IEEE, 2014, pp. 1106–1111.

[22] B. Hexsel, N. Chakraborty, and K. Sycara, "Coverage control for mobile anisotropic sensor networks," in *2011 IEEE International Conference on Robotics and Automation*. IEEE, 2011, pp. 2878–2885.

[23] P. Konstantinova, A. Udvarev, and T. Semerdjiev, "A study of a target tracking algorithm using global nearest neighbor approach," in *Proceedings of the International Conference on Computer Systems and Technologies (CompSysTech'03)*, 2003, pp. 290–295.

[24] S. Hamid Rezatofighi, A. Milan, Z. Zhang, Q. Shi, A. Dick, and I. Reid, "Joint probabilistic data association revisited," in *Proceedings of the IEEE International Conference on Computer Vision*, 2015, pp. 3047–3055.

[25] S. S. Blackman, "Multiple hypothesis tracking for multiple target tracking," *IEEE Aerospace and Electronic Systems Magazine*, vol. 19, no. 1, pp. 5–18, 2004.

[26] A. Doucet, B.-N. Vo, C. Andrieu, and M. Davy, "Particle filtering for multi-target tracking and sensor management," in *Proceedings of the Fifth International Conference on Information Fusion. FUSION 2002.(IEEE Cat. No. 02EX5997)*, vol. 1. IEEE, 2002, pp. 474–481.

[27] R. P. Mahler, "Multitarget bayes filtering via first-order multitarget moments," *IEEE Transactions on Aerospace and Electronic systems*, vol. 39, no. 4, pp. 1152–1178, 2003.

[28] P. M. Dames, "Distributed multi-target search and tracking using the PHD filter," *Autonomous Robots*, pp. 1–17, 2019.

[29] B.-N. Vo, S. Singh, A. Doucet, *et al.*, "Sequential Monte Carlo implementation of the PHD filter for multi-target tracking," in *Proc. Int'l Conf. on Information Fusion*, 2003, pp. 792–799.

[30] P. Dames and V. Kumar, "Experimental characterization of a bearing-only sensor for use with the PHD filter," *arXiv preprint arXiv:1502.04661*, 2015.

[31] F. Aurenhammer, "Power diagrams: properties, algorithms and applications," *SIAM Journal on Computing*, vol. 16, no. 1, pp. 78–96, 1987.

[32] D. Schuhmacher, B.-T. Vo, and B.-N. Vo, "A consistent metric for performance evaluation of multi-object filters," *IEEE Transactions on Signal Processing*, vol. 56, no. 8, pp. 3447–3457, 2008.

[33] H. W. Kuhn, "The Hungarian method for the assignment problem," *Naval Research Logistics Quarterly*, vol. 2, no. 1-2, pp. 83–97, 1955.